Optik 148 (2017) 54–62

Contents lists available at ScienceDirect

Optik

journal homepage: www.elsevier.de/ijleo

Original research article

Investigation of highly efficient methyl ammonium lead halide perovskite solar cell with non-textured front surface

S.M. Iftiquar[a,*], Jung Soo Kim[a], Junsin Yi[a,b,*]

[a] College of Information and Communication Engineering, Sungkyunkwan University, Suwon 440-746, Republic of Korea
[b] Department of Energy Science, Sungkyunkwan University, Suwon 440-746, Republic of Korea

ARTICLE INFO

Article history:
Received 22 May 2017
Received in revised form 17 August 2017
Accepted 28 August 2017

Keywords:
Methyl ammonium lead halide perovskite
Solar cell
Optical absorption
Device efficiency

ABSTRACT

High quality methyl ammonium lead iodide ($MAPbI_3$) perovskite material based single junction solar cell was investigated by simulation. We observed a systematic variation in device performance due to a variation in optical absorption of the active layer. By changing thickness of absorber layer from 50 nm to 1000 nm, we obtained power conversion efficiency (PCE) of the photovoltaic devices varying from 7.9% to 21.1%. Its open circuit voltage (V_{oc}) varied from 1.26 V to 1.16 V, short circuit current density (J_{sc}) varied from 7.56 mA/cm^2 to 22.61 mA/cm^2 while the fill factor (*FF*) remained constant at 83% in this variation. Front surface of the solar cell was kept non-textured, however, back reflection of unabsorbed light was used in the analysis. The maximum PCE of 21.1% and J_{sc} of 22.61 mA/cm^2 was observed for the solar cell with 1000 nm absorber layer. The J_{sc} and device efficiency increases with increased thickness of absorber layer (d_i). Therefore, higher PCE can be obtained with a thicker absorber layer. However, we identify that, with 94 nm thick absorber layer, the rate of change of PCE is equal to the rate of change of J_{sc}, due to the thickness variation. In this cell with 94 nm thick absorber layer (Cell-94), the PCE was 11.5%, nearly half of the PCE obtained with 1000 nm absorber layer. In the Cell-94, the diode ideality factor was 2.04, and reverse saturation current density was 6×10^{-13} Amp/cm^2.

1. Introduction

Recent development in methyl ammonium lead iodide ($MAPbI_3$) perovskite material has drawn intense interest to explore its potential in fabricating photovoltaic (PV) solar cell. Apart from the iodide [1–3] $MAPbI_3$, its chloride [4], bromide [5] and mixed halides [6] were also investigated. Among the various halide perovskites the iodide one shows attractive optical absorption [7], carrier mobility (500–800 cm^2 volt^{-1} s^{-1} [8]), diffusion length [9,10], high lifetime [11,12] that can be even more than 15 μs [13], photo sensitivity and device performance [14–16]. These perovskite materials have superior optoelectronic properties than thin film amorphous silicon semiconductors. A simple preparation technique [17–19], superior crystallinity [20,21] and optoelectronic properties are few of the attractive features that invited various research groups to explore the material for solar photovoltaics. A number of theoretical [22–25], experimental investigations [1–21,26,27] and review work [28–31] were also carried out to understand and explore its photovoltaic capabilities. It was reported that a careful preparation of material and device fabrication can lead to a larger crystallite grain size [20], lower defect density

* Corresponding authors at: College of Information and Communication Engineering, Sungkyunkwan University, Suwon, 440-746, Republic of Korea.
E-mail addresses: iftiquar@skku.edu (S.M. Iftiquar), junsin@skku.edu (J. Yi).

http://dx.doi.org/10.1016/j.ijleo.2017.08.141
0030-4026/

[32,33] and higher device efficiency [8]. Even though these materials are prepared in a simple technique, yet its defect density remains remarkably low.

However, this material is not free from its limitations. Degradation is one of the most important aspects of the device. It is thought that due to poor thermal conductivity of this material, the heat inside the perovskite material may create thermal stress [34], due to which ionic migration [33,34] within the bulk material leads to vacancy related defects [35]. In that respect a thinner perovskite layer may help in avoiding such a rapid degradation. Therefore, most of the experimental researches are limited to thinner perovskite layer. Ferro-electric hysteresis [36,37] is another effect that bring uncertainty to the experimental measurements. It was reported that a faster or slower scan rate [38], forward or reverse voltage scan [10,39], can change the current density- voltage (J-V) characteristic curve significantly, thereby the experimental error can mask the actual device characteristics. A standardized scan (0.01 V/sec [38]) or voltage sweep rate can reduce such an error. Furthermore, errors in experimental investigation is not very uncommon. For example, in reference [7], experimental results on open circuit voltage (V_{oc}), short-circuit current density (J_{sc}), fill factor (*FF*) and power conversion efficiency (PCE) of perovskite solar cells shows variable measurement errors, as well as trend of variation is not very clear.

In order to systematically explore performance characteristics of such an organic-inorganic halide $MAPbI_3$ perovskite solar cell, we used numerical simulation, where the experimental errors are avoidable and a systematic device characteristics can be explored. We used a simple device structure, with indium tin oxide (ITO) as front electrode, TiO_2 as electron transporting layer (ETL), $MAPbI_3$ as photo-sensitive active layer, and Spiro-MeOTAD as hole transporting layer (HTL) [40,41] and gold (Au) as back electrode. Although ZnO can also be used as ETL [42]. Even though the energy levels of the valence and conduction bands of the materials depends upon preparation condition and may require additional buffer layers, yet we investigated the devices without such buffer layers. Although, it can be predicted theoretically that a thicker absorber layer can generate more electron-hole pairs, therefore increased J_{sc} and efficiency can be achieved, however, in practice, several other inter-dependant parameters may act against such a trend to mask the expected high efficiency. Therefore, simulation or theoretical results can be considered as experimentally achievable limiting values. In this article we report our investigation of structure of a perovskite solar cell where efficient photovoltaic conversion takes place.

2. Theoretical

Photovoltaic energy is generated after absorption of light in solar cell. The light absorption ($I\left(\lambda\right)$) in active layer of a solar cell creates energetic electron-hole pairs that should be separated before recombination. The light absorption, in a layer of thickness *d* and absorption coefficient α, follows Beer Lambert's exponential relation

$$I\left(\lambda\right) = I_0\left(\lambda\right)\left(1 - e^{-\alpha d}\right) \tag{1}$$

here $I_0\left(\lambda\right)$ is the spectral distribution of incident light, λ is wavelength. This means, a thicker layer and material of higher absorption coefficient can have higher optical absorption. Total light absorption can be expressed by integrating the Eq. (1). The integrated light absorption (Abs_1) and J_{sc} are known to be related as follows:

$$J_{sc} = A_1 q \int_{\lambda 1}^{\lambda 2} I(\lambda)\, d\lambda = A_1 q Abs_1 \tag{2}$$

Here A_1 is a constant related to external quantum efficiency (EQE), $I(\lambda)$ is spectral distribution of absorbed light, the integration range (λ1, λ2) is the wavelength range that dominantly contribute to J_{sc} or photovoltaic energy generation. Here

$$Abs_1 = \int_{\lambda 1}^{\lambda 2} I(\lambda)\, d\lambda \tag{3}$$

The photo-generated carriers are separated by the ETL and HTL layers. However, all these carriers cannot be collected, as some of them are lost by Shockley-Read-Hall type defect mediated recombination ($E_{L(SRH)}$), Auger recombination (E_{Auger}) and band to band recombination (E_{BB}). This carrier separation and recombination in a PV device depends on various factors like thickness and opto-electronic properties of the materials. In addition to the electronic loss, optical loss ($E_{L(opt)}$) also plays a significant role in device performance. It depends upon optical design of the device, for example, introducing texturing at the front surface will reduce reflection loss of incident light, therefore $E_{L(opt)}$ will become lower. Few of the major optical loss channels are, reflection at the front surface, parasitic absorption at the ETL, HTL layers, transmission loss of unabsorbed light. The $E_{L(opt)}$ can significantly be reduced by using light trapping structure, in which reflection at the front surface is reduced and the transmitted light are reflected back to solar cell for further absorption. If E_{in} is energy of incident light and E_{out} is output electrical energy from a PV device and E_{Loss} is sum of other possible loss mechanisms, then cell output electrical energy can approximately be expressed as:

$$E_{out} = E_{in} - E_{L(opt)} - E_{L(SRH)} - E_{Auger} - E_{BB} - E_{Loss} \tag{4}$$

This expression (4) indicates that any kind of loss mechanism can degrade output power from the device. Here E_{in} is constant incident light, $E_{L(opt)}$ is another constant, however, the recombination losses can vary, as discussed later. The Fig. 1

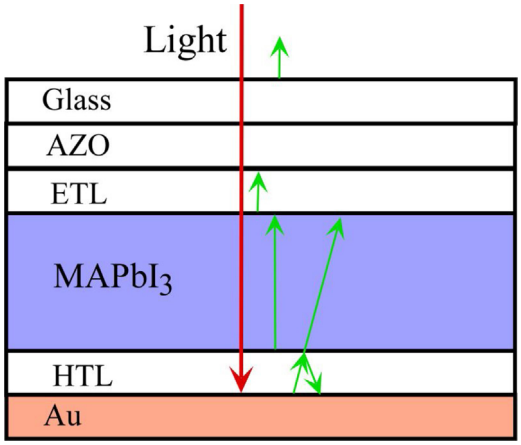

Fig. 1. Schematic diagram of a perovskite solar cell used in the investigation with device strauctre: Glass/AZO/TiO_2/$MAPbI_3$/Spiro-MeOTAD/Au, here AZO represents aluminum doped zinc oxide and Au represents gold, longest downward arrow indicates incident light. The green colored smaller arrows indicate significant light reflection at interfaces, although the reflection will take place at all the interfaces. (For interpretation of the references to colour in this figure legend, the reader is referred to the web version of this article.)

shows a schematic diagram of light travel and significant reflection at various interfaces, as it travels across the device. Although there will be reflection at each of the interfaces, but other reflections can be ignored, assuming they are small.

When carriers are generated, they can diffuse from higher concentration of carriers to lower concentration. A bending or gradient in energy levels of conduction and valence band density of states create electric field, because of which the carriers can be drifted in energetically favorable direction. Furthermore, as described above, the excess electrons and holes, generated by incident light can be partly lost by recombination. This combination of generation, recombination and drift-diffusion of electron-hole pairs are exhibited in a solar cell as its output characteristics. Therefore, theoretically combining these processes, one can simulate characteristics of a solar cell under various conditions. Such a numerical solution is suitably implemented in AFORS-HET simulation program [43]. We use this program to simulate the J-V characteristics of the PV devices. Optical absorption of the absorber layers were varied by using different thickness of the perovskite absorber layer (d_i) of the cell and keeping other device parameters unchanged.

In order to simplify our investigation, textured front surface was not taken into account in the analysis. Furthermore, the textured surface may introduce surface defects [44], difficulty in preparing uniform layers etc. Although textured surface helps in light trapping and enhancement in device performance, under certain condition, the effect of surface texturing can be analyzed by using a suitable multiplying factor [45–47], therefore such a textured surface was also not used in the present investigation.

3. Simulation details

We investigated $MAPbI_3$ perovskite solar cell, with transparent titanium dioxide (TiO_2) as ETL and Spiro-MeOTAD (2,2′,7,7′,-tetrakis(N,N-di-p-methoxyphenylamino)-9,9′-spirobifluorene or $C_{81}H_{68}N_4O_8$) as HTL. The complete device structure is Au/Spiro-MeOTAD(90 nm)/$MAPbI_3$(50–1000 nm)/TiO_2(90 nm)/AZO(500 nm). Experimentally, as larger crystalline grain sizes are helpful for better charge transport, so investigation of perovskite layer of 1015 nm thickness was also reported [10]. In the front side, the TiO_2 and AZO also acts as a window layer as it has high transparency. Optical absorption in these layers are undesirable parasitic absorption loss, therefore thin layers are used. Similarly, the HTL or Spiro-MeOTAD is also expected to have low absorption. On the other hand, the $MAPbI_3$ perovskite layer is expected to actively absorb light to generate electrical energy. Therefore, we varied d_i from 50 nm to 1000 nm, so that optical absorption in this layer and hence the current density of the perovskite cell can be varied. The opto-electronic properties of the layers, used in the simulation, were taken from reference [7,23,24,48], and shown in Table 1. A good quality perovskite material will have low defect density [14,49], therefore we assumed the defect density to be 4×10^{15} cm^{-3}. Optical absorption, Abs_1, that is integrated optical absorption over concerned wavelength range, can be estimated by using Eq. (2). The J_{sc} was obtained from J-V characteristic curve of the solar cells, by simulating the device characteristicsusing AFORS-HET [43] simulation program.

4. Simulation results and analysis

The external quantum efficiency (EQE) spectra gives an indication about the absorption of solar radiation. The EQE depends on optical absorption and internal quantum efficiency (IQE). It was reported that the IQE of the cells can be close to unity [7,50]. Optical absorption at the perovskite layer depends on its internal optical absorption efficiency (IOAE). IOAE is defined similar to the IQE, without considering light reflection at the front surface or parasitic absorption at the layers other than the absorber layer. IOAE is the ratio of light absorbed by the perovskite layer, to the light entering the perovskite

Table 1
Solar cell parameters used in the AFORS-HET simulation.

Parameters	HTL	perovskite	ETL
Layer thickness (nm)	90	50–1000	90
Dielectric constant	3	30	100
Electron affinity (eV)	2.2	3.9	4
Band gap (eV)	2.9	1.5	3.2
Optical band gap (eV)	2.9	1.5	3.2
Conduction band density of states (cm^{-3})	2.5×10^{20}	2.5×10^{20}	1×10^{21}
Valence band density of states (cm^{-3})	2.5×10^{20}	2.5×10^{20}	2×10^{20}
Electron mobility ($cm^2 V^{-1} s^{-1}$)	0.0001	50	0.006
Hole mobility ($cm^2 V^{-1} s^{-1}$)	0.0001	50	0.006
Thermal velocity of holes (cm/s)	10^6	1×10^6	1×10^6
Thermal velocity of electron (cm/s)	4×10^6	1×10^6	4×10^6
Doping concentration (cm^{-3})	3×10^{18}	2.1×10^{16}	5×10^{19}
Layer density ($g\,cm^{-3}$)	2.328	2.328	2.328
Donor defect density (cm^{-3})	1×10^{16}	2×10^{14}	6.9×10^{18}
Acceptor defect density (cm^{-3})	1×10^{16}	3×10^{14}	6.9×10^{18}
Defect type	Gausian	Gaussian	Gaussian

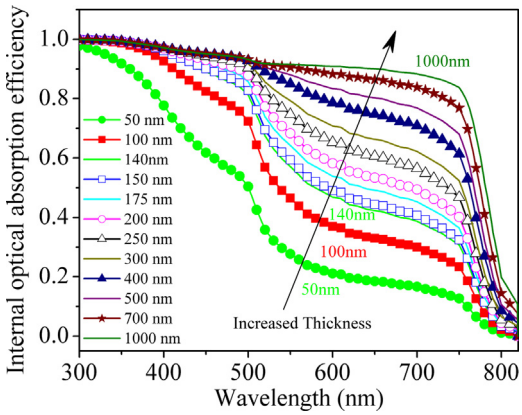

Fig. 2. Internal optical absorption efficiency (IOAE) spectra of perovskite solar cell, when thickness of the perovskite layer (d_i) was increased. The IOAE was estimated from the ratio of absorption of light in the perovskite absorber layer to the light entering the absorber layer. The direction of the arrows indicate the direction of change of the traces, when d_i was increased.

layer. Fig. 2 shows that the area under the IOAE increases with increased d_i, and the enhancement is most prominently in the longer wavelength region (~700 nm). It corresponds to the conventional concept that thicker layer is needed to absorb long wavelength radiation, as absorption coefficient of perovskite in a longer wavelength is lower. On the other hand light of wavelength shorter than 350 nm can be absorbed almost completely by an absorber layer thicker than 100 nm.

Due to variation in d_i, the light absorption in the $MAPbI_3$ absorber layer will vary. With a thicker absorber layer the IOAE of the cells increases for longer wavelength of radiation (>400 nm). This trend is easy to understand as longer wavelength radiation have lower absorption coefficient, so with a thicker absorber layer more of the longer wavelength radiation will be absorbed and the IOAE increases. The estimated EQE spectra of our devices (not shown here) are similar to Fig. 4 of Reference [7]. Integrated optical absorption (not shown here) in the absorber layer varies with thickness, d_i [24]. This can be estimated by using Eq. (2). This integrated optical absorption is related to carrier generation rate (Ge) in the perovskite absorber layer; higher optical absorption will give higher carrier generation rate. The carrier generation rate was obtained by the AFORS-HET simulation, and shown in Fig. 3. It shows that with increased d_i, the Ge increases. It can be noticed that the Ge increases sharply in the lower thickness region than that in a thicker absorber layer. This is also an indication that a stronger optical absorption takes place near the front surface of the cell, and the IOAE spectra (Fig. 2) shows that the shorter wavelength of the radiation is strongly absorbed at a shorter distance from the front surface. Therefore, longer wavelength radiation travels towards the back of the cell and gradually get absorbed when a thicker absorber layer is used. This optical absorption will create photo-generated electron-hole pairs. However, it should be mentioned here that because of recombination loss of photo generated electron-hole pairs, all these energetic charge carriers will not necessarily contribute to current generated by the cells. Therefore, we used AFORS-HET simulation to estimate current generated by these cells.

The integrated EQE is related to J_{sc}. The nature of variation of the estimated J_{sc} with increased thickness of the absorber layer, tends to reach a saturation, and varies like $\log(d_i)$ [24]. The simulated J-V curves of the solar cells are shown in Fig. 4. The solar cell device parameters, extracted from these J-V curves, are shown in Fig. 5. The variation in J_{sc} with increase in d_i, is like $\log(d_i)$, as the J_{sc} continuously increases with the d_i, but approaching towards an asymptotic limiting value. The trend in variation in J_{sc} (Fig. 5) is similar to the trend in carrier generation rate, Fig. 3. A sharp rise in J_{sc} is noticeable near the

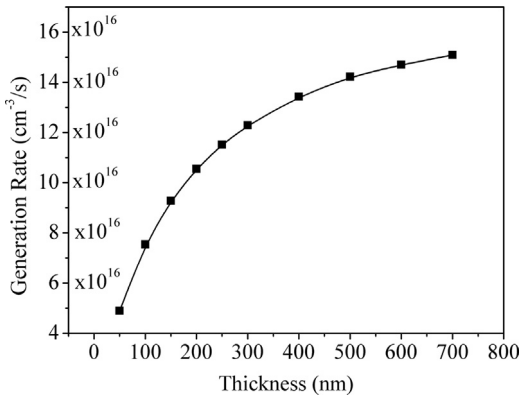

Fig. 3. Under AM1.5G insolation, variation in total carrier generation rate with thickness (d_i) of absorber layer.

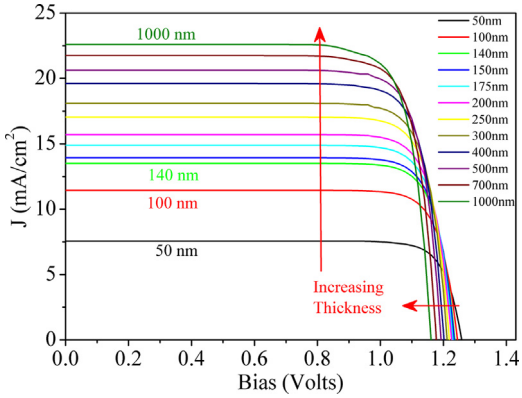

Fig. 4. Current density-voltage characteristic curves of the perovskite cell, due to variation in thickness of its active layer. The arrow in indicates the direction of change of the curves as thickness of active layer increases.

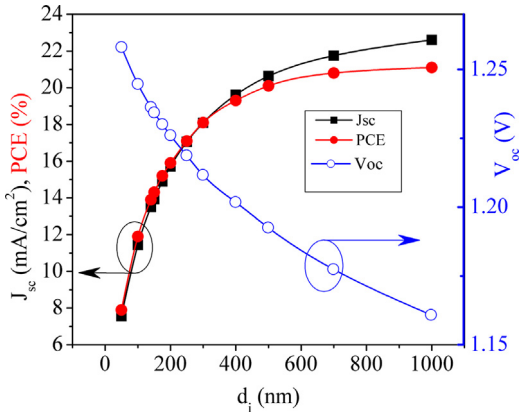

Fig. 5. Variation in V_{oc} (in blue color), J_{sc} (in black color) and power conversion efficiency or *PCE*, (in red color) of the solar cells due to the variation in thickness of the perovskite active layer. *FF* of these cells remain 83%. (For interpretation of the references to colour in this figure legend, the reader is referred to the web version of this article.)

thinner absorber layer. A steady increase in the J_{sc} with d_i indicates that a thicker absorber layer is necessary to obtain higher current density. However, until now, reports on thicker absorber layer are not very common, as thicker layers probably leads to faster degradation. Although it shows that absorption of longer wavelength of the solar radiation is important in raising current density of the device. A 21 mA/cm^2 current density was predicted for a 350 nm thick absorber layer [7], however, in our simulation we obtain 19 mA/cm^2 as short circuit current density with a similar device structure [18].

Fig. 5 shows that the V_{oc} (in blue color) decreases, J_{sc} (in black color) increases and efficiency (in red color) increases with increased optical absorption in the active layer, or d_i. Both of these variations are like log(d_i) in the sense that both the J_{sc} and efficiency increases with d_i but these parameters tend to reach an asymptotic limit. Experimentally, a 1.05 V

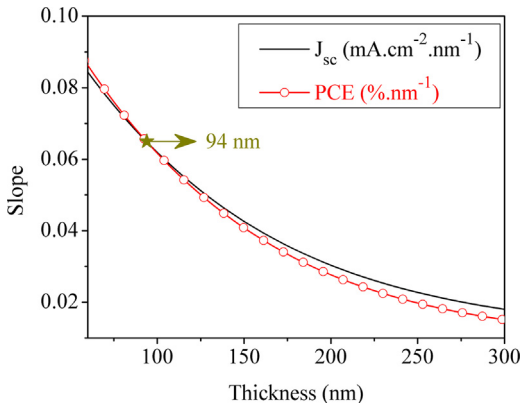

Fig. 6. Variation of slope of J_{sc} and PCE with d_i. The units of the slopes of J_{sc} and PCE are given in the legend. Here we show the plot in a 60 nm–300 nm range, that is the range of interest. The data points in PCE plot is given to clearly identify the traces. The star symbol corresponds to a point where both the slopes have equal magnitude, corresponding to d_i = 94 nm.

open circuit voltage was reported in [7], however, in our simulation we obtained 1.2 V as open circuit voltage with a similar device structure. The decrease in V_{oc} can be related to increase in total defects in the absorber layer, as thicker films will have increased number of total defects. Even though the defect density was constant but due to increase in d_i, total defects in this layer increases, leading to the fall in V_{oc}. Due to the fall in V_{oc}, the device efficiency tends to reach to saturation faster than the J_{sc}. Yet, with a very thick absorber layer, and lower defect density, higher device efficiency can be obtained, because at a lower defect density the V_{oc} will remain higher. Furthermore, it can be noticed that when d_i was 200, 250, 300 nm the J_{sc} was 15.71, 17.05, 18.09 mA/cm^2, and PCE was 15.9, 17.1, 18.1% respectively.

Carrier generation (*Ge*) and recombination rates (*Re*) are the two competing mechanisms that work in a solar cell, where higher *Ge* and lower *Re* is preferable. With the increase in d_i both the *Ge* and *Re* increases. As a result, although both the J_{sc} and PCE increases with d_i, it tends to reach a saturation. The effect of generation and recombination can be qualitatively understood from estimating rate of change of J_{sc} and PCE. Fig. 6 shows such a plot. The slope indicates rate of change with unit change in d_i. At a lower d_i the slopes for J_{sc} and PCE were high, and then these values decrease continuously with an increase in d_i. It also to be noted in Figs. 5 and 6, that with a thinner absorber layer or at a lower d_i, the rates of increase in PCE remain higher than that of J_{sc}, partly because V_{oc} also increases for thinner cells, as shown in Fig. 5. Qualitatively the higher V_{oc} and rate of change of PCE at a lower d_i, can be explained as follows. In a thinner cell, the recombination loss is less because charge carriers have to travel shorter distance.

Now, if we consider that a best cell is one where the rate of change of generation of photo-carrier becomes equal to the rate of change of PCE, then it can be expected that recombination loss of carriers will remain low with a higher PCE. This requirement may become more important in a multi junction solar cell. In a multi-junction solar cell, the optical spectra is divided in such a way that a particular subcell, predesigned for a certain wavelength range, should perform efficiently in that wavelength range [24,51]. If perovskite solar cell is used as a top subcell in a tandem device, then Fig. 6 indicates that 94 nm thick $MAPbI_3$ absorber layer is best suited. In a two-terminal perovskite-Si tandem solar cell (with two subcells), the required thickness of absorber layer of the top perovskite subcell remains higher than the 94 nm, to 140 nm [51] without surface texture or 200 nm [24] with surface texture. In a two terminal tandem solar cell, the current matching is an important aspect [24,51,52]. A similar requirement should exist in a triple junction solar cell. Therefore, it can be predicted that a triple-junction solar cell with perovskite subcell at the top, thickness of its absorber layer below or around 94 nm can produce a highly efficient device. However, in a single junction device, the problem with such a thin absorber layer is that, as our present investigation shows, the device efficiency or PCE remains lower to 11.5%, with J_{sc} as 11.1 mA/cm^2. It is also interesting to note that in a light trapping structure, 97 nm thick perovskite layer can give maximum effect of light trapping (or increase in J_{sc}), as reported in reference [24].

Carrier recombination rate (R_e) depends on various factors. In our devices we estimated the total recombination rates by using AFORS-HET simulation, and it is given in Fig. 7. In a short circuit condition, total recombination rate increases by a factor of 10 for an increase in absorber layer thickness of 153 nm.

4.1. Diode parameters

In presence of illumination, the solar cell can be considered as a diode driven by a current source (J_{sc}) [53]. In this diode equivalent model, Eq. (5), the V_{oc} is dependent on the reverse saturation current density, higher reverse saturation

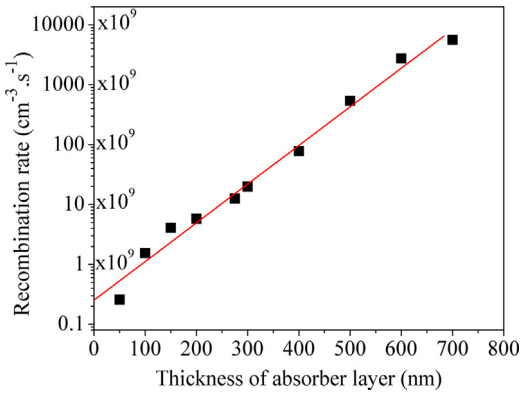

Fig. 7. Variation in recombination rate with thickness of active layer, in the short circuit condition.

current density results in a lower V_{oc} and vice versa. Therefore, we investigated the diode parameters of these cells, based on numerical solution of the diode equation.

$$J = J_{sc} - J_0\left[e^{\left(\frac{qV_b + qJR_s}{nkT}\right)} - 1\right] - \frac{V_b + JR_s}{R_p} \tag{5}$$

Here V_b is external electrical bias, R_s, R_p are series and shunt resistances, n diode ideality factor, k Boltzmann constant, T temperature.

The diode parameters of these cells were extracted using a method as described in Reference [53], and are shown in Fig. 8. It shows that the reverse saturation current density, J_0, increases with increase in d_i. It was suggested that the reverse saturation current density is related to recombination loss of carriers [53]. Fig. 7 shows that the R_e increases with the increased in d_i, and Fig. 8(a) shows that the J_0 also increases with the d_i. Although the exact nature of variation of these two parameters (R_e, J_0) differ, but the increasing trend in both the cases indicate that the J_0 is possibly related to the recombination loss. When d_i was 200 and 400 nm, the ratio of the recombination loss and the J_0 remains $\sim 10^{20}$ cm^{-1}.s^{-1} Amp^{-1}. Based on the Eq. (5), the diode ideality factor can be termed as a shielding parameter for applied voltage or electric field, so when the effective electrical bias gets reduced the n can increase. Here V_{oc} can be considered as the effective electrical bias. Furthermore, when total defects in the material increases or absorber layer becomes thicker, the electric field across this layer decreases, which is equivalent to an increase in shielding of electric field or increase in ideality factor. We observed an decrease in V_{oc} with the increase in d_i, Fig. 5. Therefore, it seems reasonable that, in Fig. 8(b) the n increases with the increase in d_i.

As discussed earlier, we identify for a cell with 94 nm thick absorber layer (Cell-94), the rate of change of PCE is equal to the rate of change of J_{sc}, due to the thickness variation. In this Cell-94, the PCE was 11.5%, nearly half of the PCE obtained with 1000 nm absorber layer, and the diode ideality factor was 2.04, and reverse saturation current density was 6×10^{-13} Amp/cm^2.

Now, considering the Eq. (4) again, we see that device efficiency increases with increased thickness of absorber layers (Fig. 5), although E_{in} was unchanged. With the increase in recombination loss, as seen in Fig. 7, it is expected that the E_{out} should decrease. Here, it is to be noted that the E_{Loss} contains unabsorbed light that transmits through the cell. With

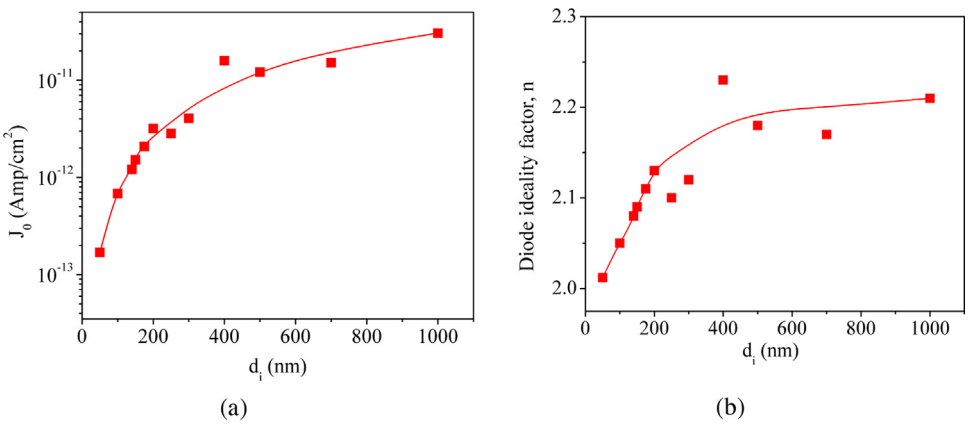

Fig. 8. Diode equivalent parameters of the solar cells under AM1.5G insolation, (a) reverse saturation current density, (b) diode ideality factor. The solid lines are drawn as an approximate mean along the data or a guide to the eye. The other parameters, like shunt and series resistances remain around 10^{18} Ω cm^2, and 10^{-15} Ω cm^2 respectively, that can be considered to have negligible influence on the J-V characteristic curves.

increased thickness, this term reduces, because of which the carrier generation rate increases, as shown in Fig. 3. A difference in the carrier generation and recombination loss is reflected as efficiency or device output, that is estimated by numerical simulation in AFORS-HET.

In this investigation we did not use textured front surface. However, a limited number of significant reflections from the interfaces were considered to estimate device characteristics. Therefore the optimized device efficiency remains lower than that is expected with a light trapping structure. An optimized textured surface [44,54], device structure and back reflector can improve device performance.

5. Conclusions

In our theoretical investigation we have observed that a higher device efficiency can be obtained with a thicker absorber layer, but the most efficient use of absorbed photon happens when thickness of absorber layer was 94 nm. Short wavelength radiation can be absorbed with a thinner absorber layer but the absorption of long wavelength radiation requires a thicker absorber layer or light trapping scheme where the thickness of the active layer can effectively be increased. In our analysis we considered partial back reflection of unabsorbed light, therefore, even with a back reflection a thicker absorber layer is required to raise current density and device efficiency. However, due to a progressive reduction in V_{oc} with an increased d_i, the enhancement in device efficiency remains lower with increased d_i. The reduction in V_{oc} is primarily due to an increase in reverse saturation current density, J_0. This situation can partially be improved by using a less defective material and using suitable buffer layers at the interfaces.

Acknowledgments

This research was supported by Basic Science Research Program through the National Research Foundation of Korea(NRF) funded by the Ministry of Education (NRF-2016R1D1A1B03935259).

This research was supported by Basic Science Research Program through the National Research Foundation of Korea(NRF) funded by the Ministry of Education(NRF-2010-0020210).

References

[1] M.M. Lee, J. Teuscher, T. Miyasaka, T.N. Murakami, H.J. Snaith, Efficient hybrid solar cells based on meso-superstructured organometal halide perovskites, Science 338 (2012) 643–647, http://dx.doi.org/10.1126/science.1228604.
[2] X. Ke, J. Yan, A. Zhang, B. Zhang, Y. Chen, Optical band gap transition from direct to indirect induced by organic content of $CH_3NH_3PbI_3$ perovskite films, Appl. Phys. Lett. 107 (2015) 091904, http://dx.doi.org/10.1063/1.4930070.
[3] A. Kojima, K. Teshima, Y. Shirai, T. Miyasaka, Organometal halide perovskites as visible-light sensitizers for photovoltaic cells, J. Am. Chem. Soc. 131 (2009) 6050–6051, http://dx.doi.org/10.1021/ja809598r.
[4] F.X. Xie, H. Su, J. Mao, K.S. Wong, W.C.H. Choy, Evolution of diffusion length and trap state induced by chloride in perovskite solar cell, J. Phys. Chem. C 120 (2016) 21248–21253, http://dx.doi.org/10.1021/acs.jpcc.6b06914.
[5] J.-S. Park, S. Choi, Y. Yan, Y. Yang, J.M. Luther, S.-H. Wei, P. Parilla, K. Zhu, Electronic structure and optical properties of α-$CH_3NH_3PbBr_3$ perovskite single crystal, J. Phys. Chem. Lett. 6 (2015) 4304–4308, http://dx.doi.org/10.1021/acs.jpclett.5b01699.
[6] M. Antonietta Loi, J.C. Hummelen, Hybrid solar cells: perovskites under the Sun, Nat. Mater. 12 (2013) 1087–1089, http://dx.doi.org/10.1038/nmat3815.
[7] Q. Lin, A. Armin, R.C.R. Nagiri, P.L. Burn, P. Meredith, Electro-optics of perovskite solar cells, Nat. Photon. 9 (2015) 106–112, http://dx.doi.org/10.1038/nphoton.2014.284.
[8] D.A. Valverde-Chávez, C.S. Ponseca, C.C. Stoumpos, A. Yartsev, M.G. Kanatzidis, V. Sundström, D.G. Cooke, Intrinsic femtosecond charge generation dynamics in single crystal $CH_3NH_3PbI_3$, Energy Environ. Sci. 8 (2015) 3700–3707, http://dx.doi.org/10.1039/c5ee02503f.
[9] F. Brivio, K.T. Butler, A. Walsh, M. Van Schilfgaarde, Relativistic quasiparticle self-consistent electronic structure of hybrid halide perovskite photovoltaic absorbers, Phys. Rev. B Condens. Matter Mater. Phys. 89 (2014) 155204, http://dx.doi.org/10.1103/PhysRevB.89.155204.
[10] T. Salim, S. Sun, Y. Abe, A. Krishna, A.C. Grimsdale, Y.M. Lam, Perovskite-based solar cells: impact of morphology and device architecture on device performance, J. Mater. Chem. A 3 (2015) 8943–8969, http://dx.doi.org/10.1039/c4ta05226a.
[11] D.W. DeQuilettes, S.M. Vorpahl, S.D. Stranks, H. Nagaoka, G.E. Eperon, M.E. Ziffer, H.J. Snaith, D.S. Ginger, Impact of microstructure on local carrier lifetime in perovskite solar cells, Science 348 (2015) 683–686, http://dx.doi.org/10.1126/science.aaa5333.
[12] D. Song, P. Cui, T. Wang, D. Wei, M. Li, F. Cao, X. Yue, P. Fu, Y. Li, Y. He, B. Jiang, M. Trevor, Managing carrier lifetime and doping property of lead halide perovskite by postannealing processes for highly efficient perovskite solar cells, J. Phys. Chem. C 119 (2015) 22812–22819, http://dx.doi.org/10.1021/acs.jpcc.5b06859.
[13] Y. Bi, E.M. Hutter, Y. Fang, Q. Dong, J. Huang, T.J. Savenije, Charge carrier lifetimes exceeding 15 μs in methylammonium lead iodide single crystals, J. Phys. Chem. Lett. 7 (2016) 923–928, http://dx.doi.org/10.1021/acs.jpclett.6b00269.
[14] H.A. Abbas, R. Kottokkaran, B. Ganapathy, M. Samiee, L. Zhang, A. Kitahara, M. Noack, V.L. Dalal, High efficiency sequentially vapor grown n-i-p $CH_3NH_3PbI_3$ perovskite solar cells with undoped P3HT as p-type heterojunction layer, APL Mater. 3 (2015) 016105, http://dx.doi.org/10.1063/1.4905932.
[15] N. Ahn, D.Y. Son, I.H. Jang, S.M. Kang, M. Choi, N.G. Park, Highly reproducible perovskite solar cells with average efficiency of 18.3% and best efficiency of 19.7% fabricated via lewis base adduct of lead(II) iodide, J. Am. Chem. Soc. 137 (2015) 8696–8699, http://dx.doi.org/10.1021/jacs.5b04930.
[16] L.C. Chen, J.C. Chen, C.C. Chen, C.G. Wu, Fabrication and properties of high-efficiency perovskite/PCBM organic solar cells, Nanoscale Res. Lett. 10 (2015) 312, http://dx.doi.org/10.1186/s11671-015-1020-2.
[17] V.W. Bergmann, S.A.L. Weber, F. Javier Ramos, M.K. Nazeeruddin, M. Grätzel, D. Li, A.L. Domanski, I. Lieberwirth, S. Ahmad, R. Berger, Real-space observation of unbalanced charge distribution inside a perovskite-sensitized solar cell, Nat. Commun. 5 (2014) 5001, http://dx.doi.org/10.1038/ncomms6001.
[18] J.M. Ball, M.M. Lee, A. Hey, H.J. Snaith, Low-temperature processed meso-superstructured to thin-film perovskite solar cells, Energy Environ. Sci. 6 (2013) 1739–1743, http://dx.doi.org/10.1039/c3ee40810h.
[19] H. Shen, Y. Wu, J. Peng, T. Duong, X. Fu, C. Barugkin, T.P. White, K. Weber, K.R. Catchpole, Improved reproducibility for perovskite solar cells with 1 cm2 active area by a modified two-step process, ACS Appl. Mater. Interfaces 9 (2017) 5974–5981, http://dx.doi.org/10.1021/acsami.6b13868.

[20] X. Bao, Y. Wang, Q. Zhu, N. Wang, D. Zhu, J. Wang, A. Yang, R. Yang, Efficient planar perovskite solar cells with large fill factor and excellent stability, J. Power Sources 297 (2015) 53–58, http://dx.doi.org/10.1016/j.jpowsour.2015.07.081, 21522.
[21] M.M. Rashad, A.M. Elseman, A.M. Hassan, Facile synthesis, characterization and structural evolution of nanorods single-crystalline $(C_4H_9NH_3)_2PbI_2X_2$ mixed halide organometal perovskite for solar cell application, Opt. Int. J. Light Electron Optics 127 (2016) 9775–9787, http://dx.doi.org/10.1016/j.ijleo.2016.07.054.
[22] J. Bisquert, L. Bertoluzzi, I. Mora-Sero, G. Garcia-Belmonte, Theory of impedance and capacitance spectroscopy of solar cells with dielectric relaxation, drift-diffusion transport, and recombination, J. Phys. Chem. C 118 (2014) 18983–18991, http://dx.doi.org/10.1021/jp5062144.
[23] F. Liu, J. Zhu, J. Wei, Y. Li, M. Lv, S. Yang, B. Zhang, J. Yao, S. Dai, Numerical simulation: toward the design of high-efficiency planar perovskite solar cells, Appl. Phys. Lett. 104 (2014) 253508, http://dx.doi.org/10.1063/1.4885367.
[24] S.M. Iftiquar, J. Yi, Numerical simulation and light trapping in perovskite solar cell, J. Photonics Energy 6 (2016) 025507, http://dx.doi.org/10.1117/1.JPE.6.025507.
[25] M. Mehrabian, S. Dalir, 11.73% efficient perovskite heterojunction solar cell simulated by SILVACO ATLAS software, Opt. Int. J. Light Electron Optics 139 (2017) 44–47, http://dx.doi.org/10.1016/j.ijleo.2017.03.077.
[26] M.R. Ahmadian-Yazdi, F. Zabihi, M. Habibi, M. Eslamian, Effects of process parameters on the characteristics of mixed-halide perovskite solar cells fabricated by one-step and two-step sequential coating, Nanoscale Res. Lett. 11 (2016) 408, http://dx.doi.org/10.1186/s11671-016-1601-8.
[27] M. Habibi, M.R. Ahmadian-Yazdi, M. Eslamian, Optimization of spray coating for the fabrication of sequentially deposited planar perovskite solar cells, J. Photonics Energy 7 (2017) 022003, http://dx.doi.org/10.1117/1.JPE.7.022003.
[28] P. Gao, M. Grätzel, M.K. Nazeeruddin, Organohalide lead perovskites for photovoltaic applications, Energy Environ. Sci. 7 (2014) 2448–2463, http://dx.doi.org/10.1039/c4ee00942h.
[29] M.A. Green, A. Ho-Baillie, H.J. Snaith, The emergence of perovskite solar cells, Nat. Photon. 8 (2014) 506–514, http://dx.doi.org/10.1038/nphoton.2014.134.
[30] S.D. Stranks, H.J. Snaith, Metal-halide perovskites for photovoltaic and light-emitting devices, Nat. Nanotechnol. 10 (2015) 391–402, http://dx.doi.org/10.1038/nnano.2015.90.
[31] M. Habibi, F. Zabihi, M.R. Ahmadian-Yazdi, M. Eslamian, Progress in emerging solution-processed thin film solar cells – part II: perovskite solar cells, Renewable Sustain. Energy Rev. 62 (2016) 1012–1031, http://dx.doi.org/10.1016/j.rser.2016.05.042.
[32] M. Samiee, S. Konduri, B. Ganapathy, R. Kottokkaran, H.A. Abbas, A. Kitahara, P. Joshi, L. Zhang, M. Noack, V. Dalal, Defect density and dielectric constant in perovskite solar cells, Appl. Phys. Lett. 105 (2014) 153502, http://dx.doi.org/10.1063/1.4897329.
[33] J.M. Azpiroz, E. Mosconi, J. Bisquert, F. De Angelis, Defect migration in methylammonium lead iodide and its role in perovskite solar cell operation, Energy Environ. Sci. 8 (2015) 2118–2127, http://dx.doi.org/10.1039/c5ee01265a.
[34] M. Bag, L.A. Renna, R.Y. Adhikari, S. Karak, F. Liu, P.M. Lahti, T.P. Russell, M.T. Tuominen, D. Venkataraman, Kinetics of ion transport in perovskite active layers and its implications for active layer stability, J. Am. Chem. Soc. 137 (2015) 13130–13137, http://dx.doi.org/10.1021/jacs.5b08535.
[35] W.J. Yin, T. Shi, Y. Yan, Unique properties of halide perovskites as possible origins of the superior solar cell performance, Adv. Mater. 26 (2014) 4653–4658, http://dx.doi.org/10.1002/adma.201306281.
[36] O. Almora, I. Zarazua, E. Mas-Marza, I. Mora-Sero, J. Bisquert, G. Garcia-Belmonte, Capacitive dark currents, hysteresis, and electrode polarization in lead halide perovskite solar cells, J. Phys. Chem. Lett. 6 (2015) 1645–1652, http://dx.doi.org/10.1021/acs.jpclett.5b00480.
[37] D. Bryant, S. Wheeler, B.C. O'Regan, T. Watson, P.R.F. Barnes, D. Worsley, J. Durrant, Observable hysteresis at low temperature in hysteresis free organic-inorganic lead halide perovskite solar cells, J. Phys. Chem. Lett. 6 (2015) 3190–3194, http://dx.doi.org/10.1021/acs.jpclett.5b01381.
[38] E.L. Unger, E.T. Hoke, C.D. Bailie, W.H. Nguyen, A.R. Bowring, T. Heumüller, M.G. Christoforo, M.D. McGehee, Hysteresis and transient behavior in current-voltage measurements of hybrid-perovskite absorber solar cells, Energy Environ. Sci. 7 (2014) 3690–3698, http://dx.doi.org/10.1039/c4ee02465f.
[39] H.W. Chen, N. Sakai, M. Ikegami, T. Miyasaka, Emergence of hysteresis and transient ferroelectric response in organo-lead halide perovskite solar cells, J. Phys. Chem. Lett. 6 (2015) 164–169, http://dx.doi.org/10.1021/jz502429u.
[40] J.C. Brauer, Y.H. Lee, M.K. Nazeeruddin, N. Banerji, Charge transfer dynamics from organometal halide perovskite to polymeric hole transport materials in hybrid solar cells, J. Phys. Chem. Lett. 6 (2015) 3675–3681, http://dx.doi.org/10.1021/acs.jpclett.5b01698.
[41] E. Karimi, S.M.B. Ghorashi, Investigation of the influence of different hole-transporting materials on the performance of perovskite solar cells, Opt. Int. J. Light Electron Optics 130 (2017) 650–658, http://dx.doi.org/10.1016/j.ijleo.2016.10.122.
[42] M. Hatamvand, S.A. Mirjalili, M. Sharzehee, A. Behjat, M. Jabbari, M. Skrifvars, Fabrication parameters of low-temperature ZnO-based hole-transport-free perovskite solar cells, Opt. Int. J. Light Electron Optics 140 (2017) 443–450, http://dx.doi.org/10.1016/j.ijleo.2017.02.101.
[43] R. Stangl, J. Haschke, C. Leendertz, Numerical simulation of solar cells and solar cell characterization methods: the open-source on demand program AFORS-HET, version 2.4, in: R.D. Rugescu (Ed.), SolarEnergy, Intech, Croatia, 2009, p. 432.
[44] H. Park, S.M. Iftiquar, H.W. Kim, J. Lee, A.H.T. Le, J. Yi, Diffused transmission and texture-induced defect with transparent conducting oxide front electrode of amorphous silicon solar cell, Semicond. Sci. Technol. 28 (2013) 115012, http://dx.doi.org/10.1088/0268-1242/28/11/115012.
[45] S.M. Iftiquar, J. Jung, C. Shin, H. Park, J. Park, J. Jung, J. Yi, Light management for enhanced efficiency of textured n-i-p type amorphous silicon solar cell, Energy Mater. Sol. Cells. 132 (2014) 348–355, http://dx.doi.org/10.1016/j.solmat.2014.09.011.
[46] S.M. Iftiquar, J. Jang, H. Park, C. Shin, J. Park, J. Jung, S. Kim, J. Yi, Analysis of optical absorption and quantum efficiency due to light trapping in a n-i-p type amorphous silicon solar cell with textured back reflector, Phys. Status Solidi A Appl. Mater. Sci. 211 (2014) 924–931, http://dx.doi.org/10.1002/pssa.201330291.
[47] S.M. Iftiquar, J. Jung, H. Park, J. Cho, C. Shin, J. Park, J. Jung, S. Bong, S. Kim, J. Yi, Effect of light trapping in an amorphous silicon solar cell, Thin Solid Films 587 (2015) 117–125, http://dx.doi.org/10.1016/j.tsf.2015.02.037.
[48] C. Eames, J.M. Frost, P.R.F. Barnes, B.C. O'Regan, A. Walsh, M.S. Islam, Ionic transport in hybrid lead iodide perovskite solar cells, Nat. Commun. 6 (2015) 7497, http://dx.doi.org/10.1038/ncomms8497.
[49] J. Ye, L. Zhu, L. Zhou, X. Liu, X. Zhang, H. Zheng, G. Liu, Z. Shao, X. Pan, S. Dai, Effective and reproducible method for preparing low defects perovskite film toward highly photoelectric properties with large fill factor by shaping capping layer, Sol. Energy 136 (2016) 505–514, http://dx.doi.org/10.1016/j.solener.2016.07.034.
[50] J. Burschka, N. Pellet, S.J. Moon, R. Humphry-Baker, P. Gao, M.K. Nazeeruddin, M. Grätzel, Sequential deposition as a route to high-performance perovskite-sensitized solar cells, Nature 499 (2013) 316–319, http://dx.doi.org/10.1038/nature12340.
[51] S.M. Iftiquar, J. Junhee, Y. Junsin, Improved efficiency of perovskite-silicon tandem solar cell near the matched optical absorption between the subcells, J. Phys. D (2017), http://dx.doi.org/10.1088/1361-6463/aa8655 (Accepted for publication, 15 August 2017).
[52] J. Cho, S.M. Iftiquar, D.P. Pham, J. Jung, J. Park, S. Ahn, A.T. Le, J.S. Kim, J. Yi, Improvement in performance of tandem solar cell by applying buffer layer, back reflector and higher crystallinity of the microcrystalline Si active layer of bottom subcell, Thin Solid Films 639 (2017) 56–63, http://dx.doi.org/10.1016/j.tsf.2017.08.016.
[53] S.M. Iftiquar, J. Yi, Low reverse saturation current density of amorphous silicon solar cell due to reduced thickness of active layer, J. Electr. Eng. Technol. 11 (2016) 939–942, http://dx.doi.org/10.5370/JEET.2016.11.4.939.
[54] H. Park, S.M. Iftiquar, M. Shin, H. Kim, J. Jung, S. Kim, A.H.T. Le, Y. Kim, D.P. Pham, J.S. Jeong, J. Yi, Fabrication of honeycomb textured glass substrate and nanotexturing of zinc oxide front electrode for its application in high efficiency thin film amorphous silicon solar cell, J. Photonics Energy 7 (2017) 025502, http://dx.doi.org/10.1117/1.JPE.7.025502.